Viscous effects on Bragg scattering of water waves by an array of piles

Ali Tabaei* and Chiang C. Mei
Department of Civi & Environmental Engineering, Massachusetts Institute of Technology, Cambridge, Massachusetts 02139, USA
(Received 27 October 2008; published 25 February 2009)

We examine the effects of viscous damping in the boundary layers on the Bragg resonance of surface water waves by a two-dimensional array of vertical cylinders. For cylinders of small radius relative to the wavelength, we first derive an effective boundary condition for the radial derivative of the velocity potential to account for the viscous forces. Coupled-mode equations are then rederived by an asymptotic method for the envelopes of multiply resonated waves inside the array. Effects of viscosity on band gaps and scattering coefficients due to a plane incident wave are examined analytically for an infinitely long array of finite width surrounded by open water. For normal incidence the envelope physics is one dimensional. The transmission and reflection properties are studied first. Oblique incidence can in principle excite several wave trains in different directions. Explicit solutions are given and discussed when there are only two wave trains inside the array. Results are compared with recent theories where viscosity is not taken into account. The asymptotic theory can be modified for two-dimensional sound scattering by a cylinder array.

DOI: 10.1103/PhysRevE.79.026314 PACS number(s): 47.90.+a, 47.35.−i, 92.10.Hm, 42.79.Dj

I. INTRODUCTION

In [1,2], a theory was given for the resonant scattering of water waves by a periodic two-dimensional array of vertical cylinders standing across the depth of an open sea. The theory was motivatied by possible construction of offshsore airports consisting of a platform supported above water by vertical piles. Under the assumptions of small cylinders and large spacing comparable to a typical wavelength, a linearized theory for infinitestimal waves was studied. In particular, the cylinder spacing was assumed to be comparable to the wave length, but the cylinder radius to be small: $\mu=ka \ll 1$. Although scattering by one cylinder is weak, $O(\mu^2)$, the accumulated effects of many cylinders over a large region of length scale $O(1/k\mu^2)$ become significant when Bragg condition is nearly met. For a given lattice, the directions of the Bragg-resonated waves were first found by Ewald's construction. The evolution equations of the wave amplitudes were derived by the asymptotic method of multiple scales and were then solved for waves scattered by a infinite array of cylinders in a strip of finite width. Both normal and oblique incidence were studied. Analytical and numerical results were obtained for two and three resonant waves. Effects of band gaps on scattering characteristics were analyzed in detail.

In this article we wish to assess the effects of viscous effects in the boundary layers around the cylinders, which are unavoidable in laboratory experiments and in the field. In particular, we shall show that viscosity blurs the boundary of band gaps and hence the distinction between propagation and evanescence. In AppendixA, we give estimates to show that nonlinear effects of vortex shedding, vital for wave forces on piles in sufficiently strong waves, are not important for the weak waves considered herein. Vortex damping in large waves is likely much more important than resonant scattering and hence is a separate topic which requires a much more empirical treatment.

II. POTENTIAL FORMULATION MODIFIED FOR BOUNDARY-LAYER EFFECTS

We consider the diffraction of plane monochromatic incident waves from the open sea by a two-dimensional array of bottom-mounted vertical cylinders. The sea depth H is assumed to be constant and the radius a of the cylinders much smaller than the incident wavelength $2\pi/k$ so that $\mu=ka \ll 1$ is a small parameter. Assuming irrotationality in most of the fluid, the velocity potential outside the viscous boundary layers next to the cylinders must satisfy

$$\nabla^2\Phi + \frac{\partial^2\Phi}{\partial z^2} = 0, \quad -H \leqslant z \leqslant 0, \tag{2.1}$$

where ∇ is the gradient operator in the horizontal plane (x,y). On the sea surface, the atmospheric pressure is assumed to be constant. Restricting to infinitesimal waves, the kinematic and dynamic free surface conditions can be combined to give

$$\frac{\partial^2\Phi}{\partial t^2} + g\frac{\partial\Phi}{\partial z} = 0, \quad z = 0. \tag{2.2}$$

On the sea bed of constant depth, we have

$$\frac{\partial\Phi}{\partial z} = 0, \quad z = -H. \tag{2.3}$$

Let $\mathbf{R}(m_1,m_2)=m_1\mathbf{a}_1+m_2\mathbf{a}_2$ denote the lattice coordinate of the center of cylinder, where $(\mathbf{a}_1,\mathbf{a}_2)$ are the primitive lattice vectors in the horizontal (x,y) plane and (m_1,m_2) are integers. Let $(\mathbf{r}',z)$ be the local cylindrical polar coordinate centered at the lattice node $\mathbf{R}(m_1,m_2)$. The position of any point in space is $(\mathbf{r},z)$ with $\mathbf{r}=\mathbf{R}(m_1,m_2)+\mathbf{r}'$.

If dissipation near the cylinders is totally ignored, the boundary condition on the cylinder surface is simply

*Present address: Masdar Institute of Science and Technology, Abu Dhabi, UAE.

$$\frac{\partial \Phi}{\partial r'} = 0, \quad \forall\, r' = a. \tag{2.4}$$

It is well known for sinusoidal waves that the linearized problem can be reduced from three to two dimensions by the substitution

$$\Phi(x,y,z,t) = \phi(x,y,z)e^{-i\omega t} = \eta(x,y)Z(z)e^{-i\omega t}, \tag{2.5}$$

where η is proportional to the free-surface displacement according to

$$\zeta = \frac{i\omega\eta}{g} \tag{2.6}$$

and

$$Z(z) \equiv -\frac{ig}{\omega}\frac{\cosh k(z+H)}{\cosh kH}, \tag{2.7}$$

with $k=|\mathbf{k}|$ satisfying the dispersion relation [3]

$$\omega^2 = gk \tanh kH. \tag{2.8}$$

For brevity, we omit the symbol "Re" (real part of) for all complex expressions. The surface displacement amplitude η, which represents the horizontal pattern of $\phi(x,y,z)$, then satisfies the Helmholtz equation in the horizontal plane

$$\nabla^2\eta + k^2\eta = 0. \tag{2.9}$$

Hence for the present geometry the water-wave scattering problem is mathematically equivalent to that in two-dimensional acoustics.

The condition (2.4) is inadequate to account for viscosity, which is important in a thin boundary layer on the cylinder walls. We now find a fictitious condition within the frame of inviscid potential theory that predicts the correct force on the cylinder.

First, for a sufficiently small cylinder in relatively long waves such that $\mu=ka\ll 1$, it is well known [4] that the scattering amplitude by any one cylinder is of $O(k^2a^2)$, meaning that the disturbance to waves is weak. Outside the boundary layer, but still near a cylinder the ratio of two terms in (2.9) is $k^2\eta/\nabla^2\eta=O(k^2a^2)$; hence, η is approximately a potential—i.e.,

$$\nabla^2\eta = 0 + O(k^2a^2), \quad r' > a. \tag{2.10}$$

Without the cylinder the local velocity at the center of the cylinder and at depth z is approximately uniform horizontally. The corresponding η can be represented by

$$\eta = Ur' \cos(\theta - \theta_0), \tag{2.11}$$

where θ_0 is the direction and $U(x,y)$ the complex amplitude of $\vec{U}$, which must be solved from the analysis of waves. With the cylinder the total solution outside the boundary layer is

$$\eta = U\left(r' + \frac{a^2}{r'}\right)\cos(\theta - \theta_0). \tag{2.12}$$

Inside the oscillatory boundary layer, the tangential and transverse velocity components $(u,v)Z(z)$ are, according to Stokes theory,

$$u(r',\theta,) = -2U\sin(\theta-\theta_0)[1-e^{-(1-i)\sigma/\delta}], \tag{2.13a}$$

$$v(r',\theta) = \frac{2U}{a}\cos(\theta-\theta_0)\left[\sigma - \frac{\delta}{1-i}(1-e^{-(1-i)\sigma/\delta})\right], \tag{2.13b}$$

where $\sigma \equiv r'-a$ and $\delta=\sqrt{2\nu/\omega}$ is, the Stokes boundary layer thickness. By integrating the viscous stresses obtained from (2.13a) and (2.13b), and pressure from Bernoulli's law ($p=i\omega\rho\phi$) and (2.12), the total horizontal force per unit height of the cylinder at depth z can be found:

$$F(z) = -2\pi i\omega\rho a^2 U\left[1 + (1+i)\frac{\delta}{a}\right]Z(z), \tag{2.14}$$

which is in the direction of $\vec{U}$. The first term in the square brackets is due to inviscid pressure and the second to viscosity.

For the convenience of later analysis, let us represent the boundary layer effects by the effective (fictitious) boundary condition [5]

$$\frac{\partial\phi}{\partial r'} + \bar{\Lambda}\phi = 0, \quad r' = a, \tag{2.15}$$

which yields the same force (2.14) on the cylinder. The approximate potential satisfying (2.10) near and (2.15) on the cylinder, and approaching (2.11) at $r' \gg a$, is readily found to be

$$\phi \cong U\left(r' + \frac{a^2}{r'}\frac{1+\bar{\Lambda}a}{1-\bar{\Lambda}a}\right)\cos(\theta-\theta_0)Z(z). \tag{2.16}$$

It will be shown shortly that $\bar{\Lambda}a \ll 1$, so that

$$\phi \cong U\left(r' + \frac{a^2}{r'}(1+2\bar{\Lambda}a)\right)\cos(\theta-\theta_0)Z(z). \tag{2.17}$$

With this result the dynamic pressure on the cylinder wall is

$$p|_{r'=a} = i\omega\rho\phi|_{r'=a} \cong 2ia\omega\rho U(1+\bar{\Lambda}a)\cos(\theta-\theta_0), \tag{2.18}$$

which gives the following amplitude of the horizontal force on the cylinder:

$$F = \int_0^{2\pi} d\theta ap\cos\theta \cong -2\pi i\omega\rho a^2 U(1+\bar{\Lambda}a). \tag{2.19}$$

By equating (2.14) and (2.19), the dimensionless coefficient $\bar{\Lambda}a$ is found:

$$\bar{\Lambda}a = (\bar{\Lambda}_r + i\bar{\Lambda}_i)a = (1+i)\frac{\delta}{2a} = (1+i)\frac{1}{a}\sqrt{\frac{\nu}{2\omega}}, \tag{2.20}$$

which is a complex constant. Let us estimate the rough magnitudes of $\bar{\Lambda}a$ for water waves [6]. In the field, the following values are representative: $a\sim 1-5$ m and $ka\sim 0.1$. Let the boundary layer be turbulent and the eddy viscosity be 100

times that of the molecular viscosity—i.e., $\nu=10^{-4}$ m^2/s; then, $\bar{\Lambda}a\sim\bar{\Lambda}_r a\sim\bar{\Lambda}_i a\sim 0.01-0.002$ and is small. For laboratory experiments, $a\sim 2.5$ cm, $\omega\sim 5$ rad/s, and the kinematic viscosity at 20 °C $\nu=1\times10^{-2}$ cm^2/s, we get $\bar{\Lambda}a\sim 0.0125$, which is also small. In view of these estimates, we shall write in subsequent analysis $\bar{\Lambda}=\mu^2\Lambda$, with $\mu=ka\ll 1$ and $\Lambda=O(1)$. From here on, we shall solve (2.1) subject to the boundary conditions (2.2) and (2.3) and

$$\frac{\partial\phi}{\partial r'}+\mu^2\Lambda\phi=0,\quad r'=a,\quad \Lambda a=(\Lambda_r+i\Lambda_i)a=(1+i)\frac{\delta}{2\mu^2 a}. \tag{2.21}$$

Returning to the wave problem, it is known that scattering by each small cylinder is weak $[O(\mu^2)]$. However, when the number of cylinders in any direction is large $[O(1/\mu^2)]$, the accumulated effects may become of $O(1)$ if the Bragg resonance condition is met. In that case there are two contrasting length scales: $1/k$ and $1/\mu^2 k$. If small frequency detuning exists, there are also two contrasting time scales: $O(1/\omega)$ and $1/\mu^2\omega$. It is therefore natural to employ the asymptotic method of multiple scales. Perturbation equations are derived for the short-scale variations in each unit cell. Solvabilty of a higher-order cell problem will lead to the equations governing large-scale dynamics. Since the full analysis is quite similar to the inviscid theory of [2], many details are omitted here and only new parts will be decribed.

III. MULTIPLE-SCALE ANALYSIS AND THE FIRST-ORDER CELL PROBLEM

We shall consider a periodic array over an area much greater than the typical wavelength. Except in the immediate neighborhood of the cylinders, the wave (outer) problem is one of two contrasting scales. As in [2], we introduce fast and slow variables

$$x,y,z,t;\quad (X,Y,T)=\mu^2(x,y,t), \tag{3.1}$$

so that x, y, z, and t describe the fast motion characterized by the length and time scales of $1/k$ and $1/\omega$, while X, Y, and T describe the slow variation of the envelope over the whole array. On the short scale of a unit (periodic) cell or a wavelength, the total array is practically infinite in extent. We shall apply Bloch theorem [7,8] so that for any lattice vector $\mathbf{R}=\mathbf{R}(m_1,m_2)$,

$$\eta(\mathbf{r})=e^{i\mathbf{k}\cdot\mathbf{R}}\eta(\mathbf{r}+\mathbf{R})\quad\text{or}\quad \phi(\mathbf{r},z)=e^{i\mathbf{k}\cdot\mathbf{R}}\phi(\mathbf{r}+\mathbf{R},z) \tag{3.2}$$

with η and ϕ being horizontally periodic.

Let us expand the outer potential as follows:

$$\Phi=[\phi_1+\mu^2\phi_2+O(\mu^4)]e^{-i\omega t}, \tag{3.3}$$

where ϕ_1 and ϕ_2 are functions of $(x,y,z;X,Y,T)$. Substituting (3.3) into the governing equations (2.1)–(2.3), we obtain the governing equations for the perturbation potentials ϕ_1 and ϕ_2.

In particular, ϕ_1 only satisfies the homogeneous conditions on the fast scale in a unit cell V as sketched in Fig. 1:

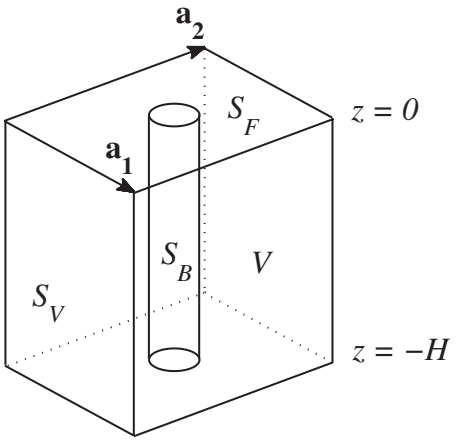

FIG. 1. A periodic cell around a vertical cylinder. $\mathbf{a}_1$ and $\mathbf{a}_2$ are the primitive lattice vectors.

$$\nabla^2\phi_1+\frac{\partial^2\phi_1}{\partial z^2}=0,\quad \text{in } V, \tag{3.4}$$

$$\frac{\partial\phi_1}{\partial z}-\frac{\omega^2}{g}\phi_1=0,\quad z=0, \tag{3.5}$$

$$\frac{\partial\phi_1}{\partial z}=0,\quad z=-H. \tag{3.6}$$

Note that these differential equations describe variations over the fast (short) scale and are the same from one periodic cell to another. The total domain $(kX,kY)=O(1)$ being very large relative to the fast coordinates, we impose Bloch condition (3.2) on ϕ_1.

Because the cylinders are so small, condition (2.21) is not effective at this order.

We assume that N progressive plane waves satisfy (or nearly satisfy) the Bragg condition of resonance. Let $\mathbf{k}_1$ denote the incident wave vector and $\mathbf{k}_j=k(\cos\beta_j,\sin\beta_j)$, $j=2,3,\ldots,N$, the resonantly scattered wave vectors, where β_j denotes the direction of $\mathbf{k}_j$ with respect to the x axis. Let $\mathbf{K}_{1,j}$ be the reciprocal lattice vector pointing from the tip of $\mathbf{k}_1$ to the tip of $\mathbf{k}_j$. The Bragg condition [7,8] reads

$$\mathbf{k}_j=\mathbf{k}_1+\mathbf{K}_{1,j},\quad j=1,2,3,\ldots,N. \tag{3.7}$$

For a given lattice and incident wave vector, $\mathbf{k}_1$ and $\mathbf{k}_j$, $j\neq 1$, can be found by Ewald's geometrical construction [7,8].

Formally the solution for ϕ_1 is the sum of all N mutually resonating progressive waves of amplitudes $A_j(X,Y,T)$:

$$\phi_1=\sum_{j=1}^{N}A_j\psi^{(j)}(x,y,z)\equiv\sum_{j=1}^{N}A_j Z(z)e^{i\mathbf{k}_j\cdot\mathbf{r}},\quad \psi^{(j)}=Z(z)e^{i\mathbf{k}_j\cdot\mathbf{r}}. \tag{3.8}$$

The slow variations of $A_j(X,Y,T)$ remain to be found at the next order.

IV. SECOND-ORDER PROBLEM

At second order, ϕ_2 is governed by

$$\nabla^2\phi_2 + \frac{\partial^2\phi_2}{\partial z^2} = -2\bar{\nabla}\cdot\nabla\phi_1, \quad \text{in } V, \tag{4.9}$$

where $\bar{\nabla} \equiv (\partial_X, \partial_Y)$,

$$\frac{\partial\phi_2}{\partial z} - \frac{\omega^2}{g}\phi_2 = \frac{2i\omega}{g}\frac{\partial\phi_1}{\partial T}, \quad z = 0, \tag{4.10}$$

$$\frac{\partial\phi_2}{\partial z} = 0, \quad z = -H. \tag{4.11}$$

Bloch condition (3.2) also applies to ϕ_2. On the cylinder surface, condition (2.21) now requires

$$\frac{\partial\phi_2}{\partial r'} = -\frac{1}{\mu^2}\frac{\partial\phi_1}{\partial r'} - \Lambda\phi_1, \quad r' = |\mathbf{r}'| = a. \tag{4.12}$$

These inhomogeneous equations govern ϕ_2 over the short coordinates in a periodic cell.

Equation (4.12) requires that the $O(1)$ gradient $\partial\phi_1/\partial r'$ on the small cylinder must be canceled by the large gradient of a small $[O(\mu^2)]$ potential. Thus ϕ_2 must change quickly in the neighborhood of $r' = O(a)$, which is much smaller than the cell size $\sim O(1/k)$. This requirement is outside the realm of (4.9)–(4.11) and (3.2) We now let ϕ_2 to be the sum of the outer and inner solutions: ϕ_2^{out} and ϕ_2^{in}. The outer solution is dominant in the far field, $\phi_2 \approx \phi_2^{\text{out}}$, $kr = O(1)$, and satisfies (4.9)–(4.11) and (3.2). On the other hand, the inner solution is of local importance and dominant in the near field only: $\phi_2 \approx \phi_2^{\text{in}}$, $r' = O(a)$. It must vanish at $O(1/k) \gg r' \gg a$, while its radial gradient must be so large as to satisfy (4.12). In this small neighborhood, ϕ_2^{in} needs only satisfy the horizontal Laplace equation instead of (4.9), with an error of μ^2. By using the approximation of $\partial\phi_1/\partial r'$ on the cylinder described in detail in [2], (4.12) becomes, approximately,

$$\frac{\partial\phi_2^{\text{in}}}{\partial r'} = -Z(z)\sum_{j=1}^{N} kA_j e^{i\mathbf{k}_j\cdot\mathbf{R}_{m_1,m_2}}\left\{\frac{i\cos(\varphi-\beta_j)}{\mu^2} - \frac{1+\cos 2(\varphi-\beta_j)}{2\mu} + \frac{\Lambda a}{\mu} + O(\mu^0)\right\}, \quad r' = a, \tag{4.13}$$

where the last term involving Λ is new. It is now easy to find the approximate solution

$$\phi_2^{\text{in}} = Z(z)\sum_{j=1}^{N} A_j e^{i\mathbf{k}_j\cdot\mathbf{R}(m_1,m_2)}\left\{\frac{\ln kr'}{2}(1-2\Lambda a) + \frac{\mathrm{i}}{\mu}\frac{a}{r'}\cos(\varphi-\beta_j) - \frac{1}{4}\frac{a^2}{r'^2}\cos 2(\varphi-\beta_j)\right\} + O(\mu). \tag{4.14}$$

From this, the value of ϕ_2^{in} on the cylinder $r' = a$ can be obtained. Together with the outer solution, the sum

$$\phi_2 = \phi_2^{\text{out}} + \phi_2^{\text{in}} \tag{4.15}$$

is uniformly valid everywhere in the unit cell surrounding the cylinder.

We now derive the envelope equations for A_j by examining the solvability of ϕ_2, without solving for ϕ^{out} explicitly,

A. Solvability of ϕ_2 and envelope equations

Refering to (3.8), we apply Green's identity to $\psi^{(j)*}$ and ϕ_2 over the unit cell shown in Fig. 1:

$$\int\int\int_V \left\{\phi_2\left(\nabla^2 + \frac{\partial^2}{\partial z^2}\right)\psi^{(j)*} - \psi^{(j)*}\left(\nabla^2 + \frac{\partial^2}{\partial z^2}\right)\phi_2\right\} dV = \int\int_{\partial V}\left(\phi_2\frac{\partial\psi^{(j)*}}{\partial n} - \psi^{(j)*}\frac{\partial\phi_2}{\partial n}\right) dS \tag{4.16}$$

where $\psi^{(j)*} = Z^*(z)e^{-i\mathbf{k}_j\cdot\mathbf{r}}$ denotes the complex conjugate of the leading-order potential $\psi^{(j)}$. The bounding surface of V, denoted by ∂V, consists of the free surface S_F, the cylinder surface S_B, the vertical surfaces S_V, and the sea bottom at $z = -H$. Since the governing equations for ϕ_2 (dominated by ϕ_2^{out}) are known away from the cylinders in terms of A_j, the above identity amounts to the solvability condition for the inhomogeneous boundary value problem and should give the evolution equations for the wave envelopes. Using the governing equations and the explicit solution of ϕ_2^{in} near the cylinders, all the integrals can be evaluated, leading to the evolution equations for A_j. Most of these integrals have already derived in [2]. The surface integral over the cylinder wall is slightly different. By following the steps of [2,9] we get

$$I_B = \sum_{h=1}^{N} \pi A_h[(1-2\Lambda a) - 2\cos(\beta_j - \beta_h)]\int_{-H}^{0} |Z(z)|^2 dz + O(\mu). \tag{4.17}$$

With this modification the new envelope equations are found. Letting

$$\mathbf{C}_g^{(j)} = C_g\frac{\mathbf{k}_j}{k}, \quad j = 1, \ldots, N, \tag{4.18}$$

denote the group velocity of wave j and

$$\Omega_0 = \frac{\pi C_g}{k\mathcal{A}} \tag{4.19}$$

the coupling coefficient, where $\mathcal{A}$ denotes the cross-sectional area of the cell, we obtain

$$\frac{\partial A_j}{\partial T} + \mathbf{C}_g^{(j)}\cdot\bar{\nabla}A_j = -\frac{1}{2}i\Omega_0\sum_{h=1}^{N}[(1-2\Lambda a) - 2\cos(\beta_j-\beta_h)]A_h, \quad j = 1, \ldots, N. \tag{4.20}$$

Returning to natural coordinates, the envelope equations read

which couple N_j mutually resonating waves in the array. The coupling coefficient $(ka)^2\Omega_0 = kC_g(\pi a^2/\mathcal{A})$ on the right-hand side of (4.21) is proportional to volume density of the cylinders in water. The effect of boundary layers is represented by the complex factor Λa. In open waters outside the area of cylinders, $a = 0$, (4.20) are uncoupled and reduce to

$$\frac{\partial A_j}{\partial T} + \mathbf{C}_g^{(j)} \cdot \bar{\nabla} A_j = 0, \quad j = 1, \ldots, N. \tag{4.22}$$

With viscous effects, the law of energy conservation becomes

$$\frac{\partial}{\partial T} \sum_{j=1}^{N} |A_j|^2 + \sum_{j=1}^{N} (\mathbf{C}_g^{(j)} \cdot \bar{\nabla} |A_j|^2) = -\Lambda_i a \Omega_0 \sum_{j=1}^{N} \sum_{h=1}^{N} (A_h A_j)^*. \tag{4.23}$$

As expected, the total energy is damped in the cylinder array by viscous dissipation whose rate increases with $\Lambda_i a$ and N.

In principle the system (4.20) can be used to study resonant diffraction by a large array in an area of any plan form, for which numerical techniques are needed in general. We now reexamine several examples of simple geometry studied in [1,2] in order to see the influence of viscous damping on one- and two-dimensional scattering. Specifically, we consider a long and straight strip of many rows of cylinders ($0 < X < L$, $-\infty < Y < \infty$), which may model the supporting structure of an offshore airport. The lattice is rectangular.

V. ONE-DIMENSIONAL SCATTERING

A. No Bragg resonance in an infinite array

Let the array be of infinite extent in all horizontal directions, and if no scattered wave is resonated in the cylinder array by the incident wave, then $N=1$. The envelope of the incident wave satisfies

$$\frac{\partial A_1}{\partial T} + \mathbf{C}_g^{(1)} \cdot \bar{\nabla} A_1 = \frac{1}{2} \mathrm{i} \Omega_0 (1 + 2\Lambda a) A_1, \tag{5.1}$$

which has the solution

$$A_1(X, Y, T) = A_1^0 (X \cos \beta_1 + Y \sin \beta_1 - C_g T) e^{(i\Omega_0/2)(1+2\Lambda a)T}. \tag{5.2}$$

Using (5.2), the corresponding free-surface elevation is

$$\zeta = \frac{\mathrm{i}\omega\eta}{g} = \frac{1}{2} A_1 e^{i(\mathbf{k}_1 \cdot \mathbf{r} - \omega t)} = \frac{1}{2} A_1^0 (X \cos \beta_1 + Y \sin \beta_1 - C_g T) \times e^{i\mathbf{k}_1 \cdot \mathbf{r}} e^{-i[\omega - (\mu^2 \Omega_0/2)(1+2\Lambda_r a)]t} e^{-\mu^2 \Omega_0 (\Lambda_i a) t}. \tag{5.3}$$

Thus viscosity introduces a slow damping of the incident wave as well as a small frequency shift of $\mu^2\Omega_0/2(1+2\Lambda_r a)$. Both damping and phase shift increase with viscosity. The decaying envelope still advances at the group velocity.

B. Normal incidence and Bragg scattering

Let a train of plane incident waves arrive from $X \sim -\infty$ along the X axis, so that the incident wave vector $\mathbf{k}_1$ is parallel to the rows of a rectangular array. The incidence is normal and the reflected wave is in the negative X direction so that wave propagation is one dimensional: $\mathbf{k}_1 = k\mathbf{i}$, $\mathbf{k}_2 = -k\mathbf{i}$. Bragg condition (3.7) is satisfied if

$$\mathbf{k}_1 - \mathbf{k}_2 = 2k\mathbf{i} = \mathbf{K}_{n,0} = \frac{2\pi n}{a_1}\mathbf{i} \tag{5.4}$$

where n is any positive integer and a_1 the spacing in the x direction. This problem of one-directional propagation is equivalent to Bragg scattering by a linear array along the centerline of a long channel of width a_2.

Letting $k = n\pi/a_1$, $\beta_1 = 0$, and $\beta_2 = \pi$ in (4.20), the following pair of equations for the envelopes of the incident (A_1) and reflected (A_2) waves are found:

$$\frac{\partial A_1}{\partial T} + C_g \frac{\partial A_1}{\partial X} = -\frac{1}{2} \mathrm{i} \Omega_0 (-A_1 + 3A_2) + \mathrm{i} \Omega_0 \Lambda a (A_1 + A_2), \tag{5.5a}$$

$$\frac{\partial A_2}{\partial T} - C_g \frac{\partial A_2}{\partial X} = -\frac{1}{2} \mathrm{i} \Omega_0 (3A_1 - A_2) + \mathrm{i} \Omega_0 \Lambda a (A_1 + A_2), \tag{5.5b}$$

where

$$\Omega_0 = \frac{\pi C_g}{k\mathcal{A}} = \frac{\pi C_g}{\frac{n\pi}{a_1} a_1 a_2} = \frac{C_g}{n a_2}. \tag{5.6}$$

The energy equation (4.23) takes the following form:

$$\frac{\partial}{\partial T}(|A_1|^2 + |A_2|^2) + C_g \frac{\partial}{\partial X}(|A_1|^2 - |A_2|^2) = -2\Lambda_i a \Omega_0 |A_1 + A_2|^2.$$

1. Envelope dispersion in an infinite domain

Equations (5.5a) and (5.5b) can be combined by eliminating either A_1 or A_2 to yield the complex Klein-Gordon equation

$$\left[\frac{\partial^2}{\partial T^2} - \mathrm{i}\Omega_0 (1 + 2\Lambda a) \frac{\partial}{\partial T} - C_g^2 \frac{\partial^2}{\partial X^2} + 2\Omega_0^2 (1 - 2\Lambda a) \right] \begin{pmatrix} A_1 \\ A_2 \end{pmatrix} = 0. \tag{5.7}$$

Consider the following solution in an infinite domain:

$$A_1 = A_0 e^{\mathrm{i}KX - \mathrm{i}\Omega T}, \tag{5.8}$$

where $\mu^2 K$ and $\mu^2 \Omega$ correspond to detunings of wave number and frequency. Equation (5.7) gives the dispersion relation

$$K^2 = \left(\frac{\Omega_0}{C_g} \right)^2 \left(\frac{\Omega}{\Omega_0} + 2 \right) \left(\frac{\Omega}{\Omega_0} + 2\Lambda a - 1 \right). \tag{5.9}$$

For a range of real Ω, the real and imaginary parts of the complex K are plotted in Fig. 2 for different values of the complex parameter Λa. Without dissipation, $\Lambda a = 0.0$, it is known [1] that K is purely imaginary within the band gap $-2 < \Omega/\Omega_0 < 1$, where propagation is forbidden; outside the band gap, K is purely real, so the envelopes propagate without attenuation as dispersive waves. See Fig. 2(a). In con-

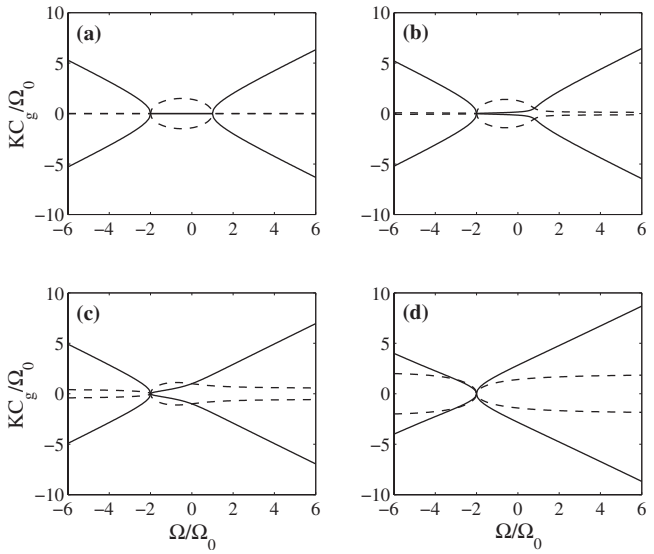

FIG. 2. Dispersion relation of water waves through infinite periodic cylinders for different values of the parameter Λa: (a) $\Lambda a=0.0$ (no dissipation), (b) $\Lambda a=0.1(1+i)$, (c) $\Lambda a=0.5(1+i)$, and (d) $\Lambda a=2.0(1+i)$. Solid curve: $\mathrm{Re}(KC_g/\Omega_0)$. Dashed curve: $\mathrm{Im}(KC_g/\Omega_0)$.

trast, with finite dissipation, K is now complex for all $\Omega/\Omega_0 \neq -2$. The band gap disappears. All waves propagate with dispersion and spatial attenuation. Larger Λa leads to stronger attenuation. At $\Omega/\Omega_0=-2$, $K=0$, the envelope is uniform in X and is infinitely long.

2. One-dimensional scattering by an array of finite width

Consider a very long array of finite width in $0 \leqslant X \leqslant L$, where $kL=O(1/\mu^2)$. The incident wave arrives from open water $x=-\infty$ normally ($\beta_1=0$) with a slight detuning from Bragg resonance and is given in the form by (5.8) where the detuning frequency and wave number are related by $\mu^2\Omega = \mu^2 C_g K$.

We expect both rightward and leftward (reflected) waves in open waters on the incidence side $X<0$ and inside the array $0<X<L$, but only rightward waves on the transmission side $X>L$. In open waters the envelopes satisfy the uncoupled equations (4.22). Inside the array we let

$$A_1 = A_0 T(X) e^{-i\Omega T}, \quad A_2 = A_0 R(X) e^{-i\Omega T}, \tag{5.10}$$

where $T(X)$ and $R(X)$ are, respectively, the local transmission and reflection coefficients in the cylinder region. It follows readily from (5.7) that T and R are governed by an ordinary differential equation of second order with constant coefficients:

$$\left(\frac{d^2}{dX^2} + m^2\right)(T,R) = 0, \tag{5.11}$$

where

$$m^2 = \frac{\Omega_0^2}{C_g^2}\left(\frac{\Omega}{\Omega_0} + 2\right)\left(\frac{\Omega}{\Omega_0} + 2\Lambda a - 1\right). \tag{5.12}$$

Thus the wave numbers are different from that in open waters. At the entrance and exit, we require the boundary conditions

$$T(0) = 1, \quad R(L) = 0. \tag{5.13}$$

The solution can be readily found:

$$T(X) = T_1 e^{imX} + T_2 e^{-imX}, \tag{5.14a}$$

$$R(X) = R_1 e^{imX} + R_2 e^{-imX}, \tag{5.14b}$$

where

$$T_1 = \frac{B+C}{(B+C)-(B-C)e^{2imL}}, \tag{5.15a}$$

$$T_2 = -\frac{(B-C)e^{2imL}}{(B+C)-(B-C)e^{2imL}}, \tag{5.15b}$$

$$R_1 = \left(\frac{3}{2} - \Lambda a\right)\frac{1}{(B+C)-(B-C)e^{2imL}}, \tag{5.16a}$$

$$R_2 = -\left(\frac{3}{2} - \Lambda a\right)\frac{e^{2imL}}{(B+C)-(B-C)e^{2imL}}, \tag{5.16b}$$

with

$$B = \frac{\Omega}{\Omega_0} + \frac{1}{2} + \Lambda a, \tag{5.17}$$

$$C = \frac{mC_g}{\Omega_0} = \sqrt{\zeta_r + i\zeta_i} = \sqrt{\frac{\sqrt{\zeta_r^2+\zeta_i^2}+\zeta_r}{2}} + i\,\mathrm{sgn}(\zeta_i)\sqrt{\frac{\sqrt{\zeta_r^2+\zeta_i^2}-\zeta_r}{2}}, \tag{5.18}$$

in which

$$\zeta_r = \left(\frac{\Omega}{\Omega_0} + 2\right)\left(\frac{\Omega}{\Omega_0} + 2\Lambda_r a - 1\right), \quad \zeta_i = \left(\frac{\Omega}{\Omega_0} + 2\right)(2\Lambda_i a). \tag{5.19}$$

In particular, the transmission coefficient at the exit is

$$T(L) = e^{-imL} + \frac{(B+C)(e^{imL} - e^{-imL})}{(B+C)-(B-C)e^{2imL}} \tag{5.20}$$

and the reflection coefficient at the entrance is

$$R(0) = \left(\frac{3}{2} - \Lambda a\right)\frac{1-e^{2imL}}{(B+C)-(B-C)e^{2imL}}. \tag{5.21}$$

The controlling parameters are Λa (viscosity), Ω/Ω_0 (detuning), and $\Omega_0 L/C_g$ (array width). For different viscosity parameters Λa, we display in Fig. 3 the spatial variation of the reflected energy intensity $|R(X)|^2$ as a function of dimensionless width of the cylinder array $\Omega_0 L/C_g$. Two detuning fre-

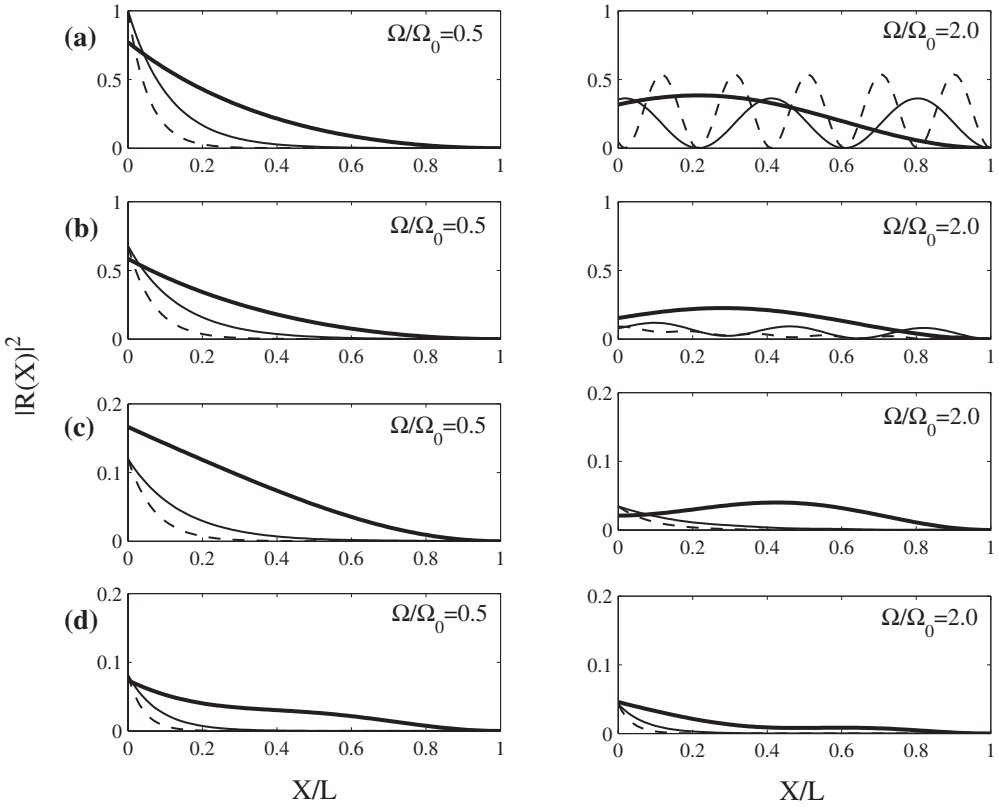

FIG. 3. Reflection intensity $|R(X)|^2$ along the lattice for various $\Omega_0 L/C_g$ with detuning parameter $\Omega/\Omega_0=0.5$ (left figures) and 2.0 (right figures) for different values of the parameter Λa: (a) $\Lambda a=0.0$ (no dissipation), (b) $\Lambda a=0.1(1+i)$, (c) $\Lambda a=0.5(1+i)$, and (d) $\Lambda a=2.0(1+i)$. Thick solid curve: $\Omega_0 L/C_g=1$. Thin solid curve: $\Omega_0 L/C_g=4$. Dashed curve: $\Omega_0 L/C_g=8$.

quencies are chosen for illustration: one inside the inviscid band gap $2<\Omega/\Omega_0<1$ with $\Omega/\Omega_0=0.5$ and one outside with $\Omega/\Omega_0=2$. For comparison we first show the results for no dissipation $\Lambda a=0.0$. Inside the band gap, $|R(X)|^2$ decays monotonically with increasing distance X from the entrance and also with increasing array width L. The reflection intensity at the entrance $R(0)$ approaches unity. Outside the band gap, $|R(X)|^2$ is oscillatory in X and vanishes along certain lines parallel to the array axis. For finite dissipation, $\Lambda a \neq 0.0$, however, $|R(X)|^2$ decays for all detuning frequencies. The attenuation is monotonic if the detuning ratio is 0.5 and is oscillatory with attenuation if the detuning is 2.0; for large enough Λa, oscillations are totally damped out. Note that there is no symmetry with respect to $\Omega/\Omega_0=-0.5$ when $\Lambda a \neq 0$.

In Fig. 4, the reflection coefficient at the entrance is plotted as a function of the dimensionless array width $\Omega_0 L/C_g$ for different degrees of dissipation Λa and for detuning $\Omega/\Omega_0=-4,-0.5,0.5,1,2$. When $\Lambda a=0.0$ and within the inviscid band gap, $-2\leqslant\Omega/\Omega_0\leqslant 1$, reflection increases monotonically and approaches unity as the array width increases. Outside the band gap, $|R(0)|^2$ is oscillatory and vanishes for certain discrete array widths. With dissipation, the bad gap disappears and $|R(0)|^2$ diminishes more rapidly in magnitude and loses oscillatory character for large $\Omega_0 L/C_g$. The distinction between propagation and evanescence disappears. In particular, windows of zero reflection for certain values of $\Omega_0 L/C_g$ become windows of weak but finite reflection.

For a few array widths $\Omega_0 L/C_g=0.5,1.0,4.0,8.0$, the dependence of reflection upon the detuning frequency is illustrated in Fig. 5. Without dissipation, reflection is very strong inside the band gap. Outside the band gap, $|R(0)|^2$ is oscillatory and vanishes at certain values of Ω/Ω_0. There is symmetry with respect to the center of the band gap, Ω/Ω_0

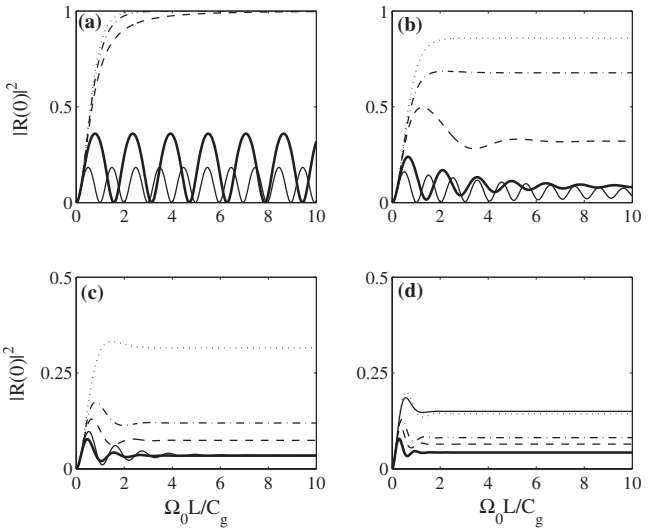

FIG. 4. Dependence of the reflection intensity at inlet $X=0$, $|R(0)|^2$, on array width $\Omega_0 L/C_g$ for various detuning parameters $\Omega/\Omega_0=-4$ (thin solid curve), -0.5 (dotted curve), 0.5 (dash-dotted curve), 1 (dashed curve), and 2 (thick solid curve) for different values of the parameter Λa: (a) $\Lambda a=0.0$ (no dissipation), (b) $\Lambda a=0.1(1+i)$, (c) $\Lambda a=0.5(1+i)$, and (d) $\Lambda a=2.0(1+i)$.

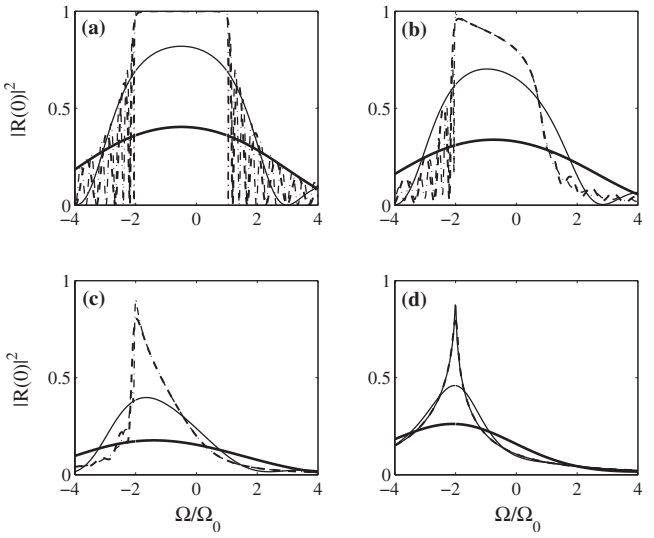

FIG. 5. Dependence of the reflection intensity at $X=0$, $|R(0)|^2$, on detuning parameter Ω/Ω_0 for various array widths $\Omega_0 L/C_g = 0.5$ (thick solid curve), 1.0 (thin solid curve), 4.0 (dashed curve), 8.0 (dashdot curve) for different values of the parameter Λa: (a) $\Lambda a = 0.0$ (no dissipation), (b) $\Lambda a = 0.1(1+i)$, (c) $\Lambda a = 0.5(1+i)$, and (d) $\Lambda a = 2.0(1+i)$.

$=-0.5$ [see Fig. 5(a)], similar to the dispersion relation shown in Fig. 2(a). When $\Lambda a \neq 0.0$, symmetry is lost. The highest reflection occurs at $\Omega/\Omega_0 = -2$. Also $|R(0)|^2$ does not vanish for any values of Ω/Ω_0 and oscillates with increasing Λa. In all cases, reflection in general decreases with increasing $|\Omega/\Omega_0|$.

VI. TWO-DIMENSIONAL SCATTERING: OBLIQUE INCIDENCE BY A LONG ARRAY

In this section we shall reexamine the simpler cases studied by [2] where only one new wave is resonantly scattered in the array—i.e., $N=2$. The case of two or more new waves $(N=3,4,\ldots)$ is algebraically more complex and is not treated here.

Without loss of generality we let the direction of the incident wave be $0 < \beta_1 < \pi/2$, so that $\mathbf{k}_1$ points to the northeast. Limiting to a square lattice, one finds by Ewald's construction that four possibilities exist for the scattered waves, as shown in Figs. 6(a)–(d) in [2]. They are the following: (i) Forward scattering: (a) $0 \leqslant \beta_2 < \pi/2$ and (b) $-\pi/2 \leqslant \beta_2 < 0$. There is in general no reflection on the left of the array, but two transmitted waves on the right. (ii) Backward scattering: (c) $\pi/2 < \beta_2 \leqslant \pi$ and (d) $\pi < \beta_2 \leqslant 3\pi/2$. There is in general reflection (hence two waves) on the left and only transmission hence one wave) on the right of the array.

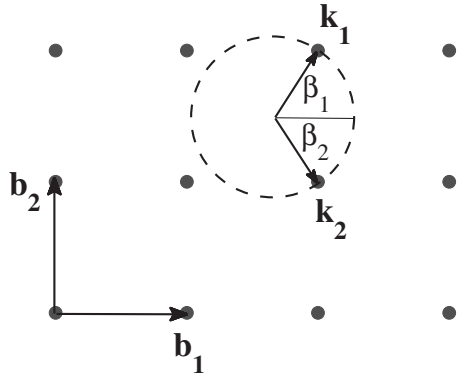

FIG. 6. Forward scattering by a square lattice of spacing a_1. The incident and scattered wave vectors $\mathbf{k}_1$ and $\mathbf{k}_2$ are inclined at $\beta_1 = \pi/3$ and $\beta_2 = -\pi/3$.

A. Solutions for wave envelopes

Inside the array, $0 \leqslant X \leqslant L$, the envelopes are denoted by A_j, $j=1,2$, which are governed by (4.20). We denote the envelopes in the open waters left of the array by A_j^- and right of the array by A_j^+, $j=1,2$, which are governed by (4.22) instead. Let the incident wave envelope be

$$A_1 = \exp[i\mathcal{K}(X\cos\beta_1 + Y\sin\beta_1) - i\Omega T],$$

$$\Omega = C_g\mathcal{K}, \quad X < 0. \tag{6.1}$$

We assume solutions of the form

$$[A_j^-, A_j, A_j^+] = A_0[B_j^-(X), B_j(X), B_j^+(X)]e^{i(\mathcal{K}\sin\beta_1 Y - \Omega T)}, \quad j = 1,2. \tag{6.2}$$

Then, inside the array, $0 < X < L$, we have

$$\frac{dB_1}{dX} = \frac{i\Omega_0}{C_g}\left\{\left[\frac{1+2\Lambda a}{2\cos\beta_1} + \frac{\Omega}{\Omega_0}\cos\beta_1\right]B_1 + \frac{2\cos(\beta_1-\beta_2) - 1 + 2\Lambda a}{2\cos\beta_1}B_2\right\}, \tag{6.3a}$$

$$\frac{dB_2}{dX} = \frac{i\Omega_0}{C_g}\left\{\frac{2\cos(\beta_1-\beta_2) - 1 + 2\Lambda a}{2\cos\beta_2}B_1 + \left[\frac{1+2\Lambda a}{2\cos\beta_2} + \left(\frac{\Omega}{\Omega_0}\right)\frac{1-\sin\beta_1\sin\beta_2}{\cos\beta_2}\right]B_2\right\}. \tag{6.3b}$$

In the open water on the left $(X<0)$, the envelopes are uncoupled:

$$\frac{dB_1^-}{dX} = i\mathcal{K}\cos\beta_1 B_1^-, \tag{6.4a}$$

$$\frac{dB_2^-}{dX} = \frac{i\mathcal{K}(1-\sin\beta_1\sin\beta_2)}{\cos\beta_2}B_2^-. \tag{6.4b}$$

On the transmission side $(X>L)$, we have instead

$$\frac{dB_1^+}{dX} = i\mathcal{K}\cos\beta_1 B_1^+, \tag{6.5a}$$

$$\frac{dB_2^+}{dX} = \frac{i\mathcal{K}(1-\sin\beta_1\sin\beta_2)}{\cos\beta_2}B_2^+. \tag{6.5b}$$

Use is made of the relation $\Omega = C_g\mathcal{K}$. Inside the array of cylinders, the envelopes are coupled:

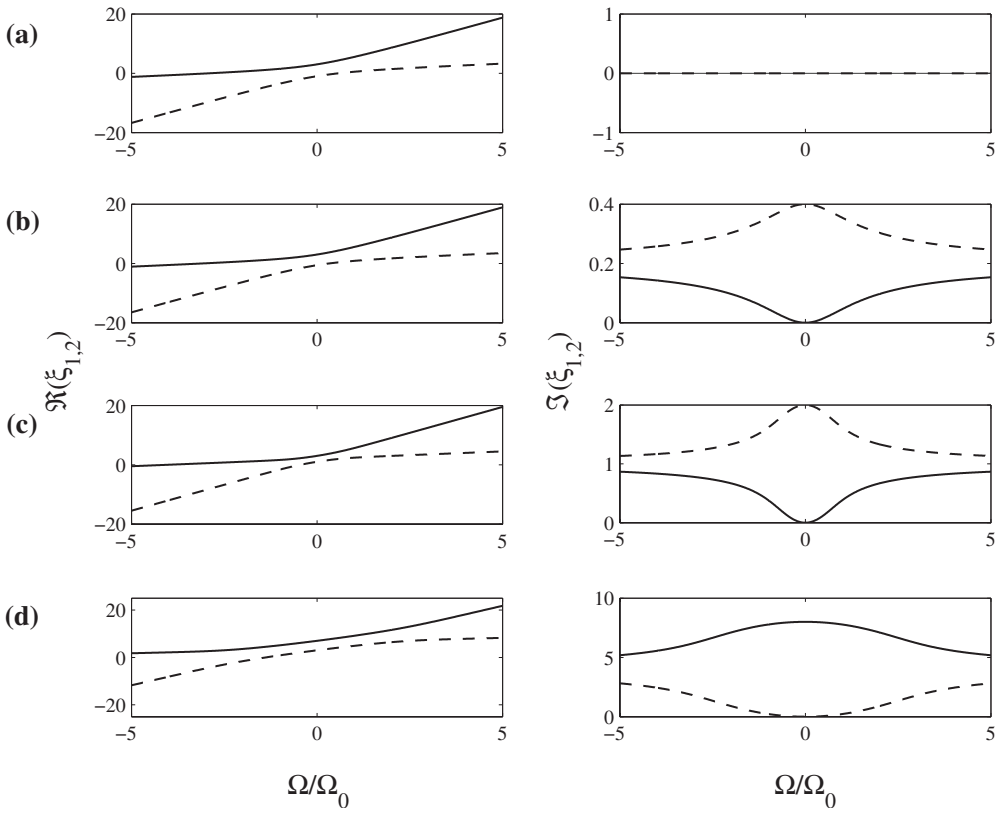

FIG. 7. Real (left) and imaginary (right) parts of the eigenvalues ξ_1 (solid curve) and ξ_2 (dashed curve) for the forward-scattering case in Fig. 6. (a) $\Lambda a=0.0$ (no dissipation), (b) $\Lambda a=0.1(1+i)$, (c) $\Lambda a=0.5(1+i)$, and (d) $\Lambda a=2.0(1+i)$. Different scales are used for the imaginary part.

$$\frac{d}{dX}\begin{bmatrix} B_1 \\ B_2 \end{bmatrix} = \frac{i\Omega_0}{C_g}\mathsf{M}\begin{bmatrix} B_1 \\ B_2 \end{bmatrix} = 0, \tag{6.6}$$

where M is the matrix with elements

$$M_{11} = \frac{1+2\Lambda a}{2\cos\beta_1} + \left(\frac{\Omega}{\Omega_0}\right)\cos\beta_1, \tag{6.7a}$$

$$M_{12} = \frac{2\cos(\beta_1-\beta_2)-1+2\Lambda a}{2\cos\beta_1}, \tag{6.7b}$$

$$M_{21} = \frac{2\cos(\beta_1-\beta_2)-1+2\Lambda a}{2\cos\beta_2}, \tag{6.7c}$$

$$M_{22} = \frac{1+2\Lambda a}{2\cos\beta_2} + \left(\frac{\Omega}{\Omega_0}\right)\frac{1-\sin\beta_1\sin\beta_2}{\cos\beta_2}. \tag{6.7d}$$

The solution is a linear combination of exponential terms

$$\begin{bmatrix} B_1 \\ B_2 \end{bmatrix} = \begin{bmatrix} b_{11} & b_{12} \\ b_{21} & b_{22} \end{bmatrix}\begin{bmatrix} E_1 \\ E_2 \end{bmatrix}, \tag{6.8}$$

where

$$E_1 = \exp\left(\frac{i\xi_1\Omega_0 X}{C_g}\right), \quad E_2 = \exp\left(\frac{i\xi_2\Omega_0 X}{C_g}\right). \tag{6.9}$$

The eigenvalues ξ_1 and ξ_2 are the roots of a quadratic equation

$$\xi_{1,2} = \frac{(M_{11}+M_{22}) \pm \Delta^{1/2}}{2}, \tag{6.10}$$

where Δ is the discriminant:

$$\begin{aligned}\Delta &= (M_{11}+M_{22})^2 - 4(M_{11}M_{22}-M_{12}M_{21}) \\ &= (M_{11}-M_{22})^2 + 4M_{12}M_{21} \\ &= \left[\frac{1+2\Lambda a}{2}\left(\frac{1}{\cos\beta_1}-\frac{1}{\cos\beta_2}\right) + \left(\frac{\Omega}{\Omega_0}\right)\frac{\cos(\beta_1-\beta_2)-1}{\cos\beta_2}\right]^2 \\ &\quad + \frac{[2\cos(\beta_1-\beta_2)-1+2\Lambda a]^2}{\cos\beta_1\cos\beta_2}.\end{aligned} \tag{6.11}$$

Since Λa is complex, both eigenvalues are always complex, implying spatial attenuation or amplification along X in addition to the oscillatory behavior. For a given lattice, we first find the direction β_2 of the scattered wave for a given incident wave $\mathbf{k}_1$ by Ewald's construction. The discriminant Δ and the eigenvalues then depend on the inclinations (β_1,β_2) and the detuning frequency Ω/Ω_0 as given by (6.10) and (6.11), which are affected by viscosity. The coefficients b_{ij} are to be determined by the matching boundary conditions at $X=0,L$, which differ among four cases described before. We now discuss two cases.

B. Forward scattering: $\cos\beta_2>0$

We shall only study one of the two cases where the scattered wave is directed to the south-east, as shown in Fig. 6.

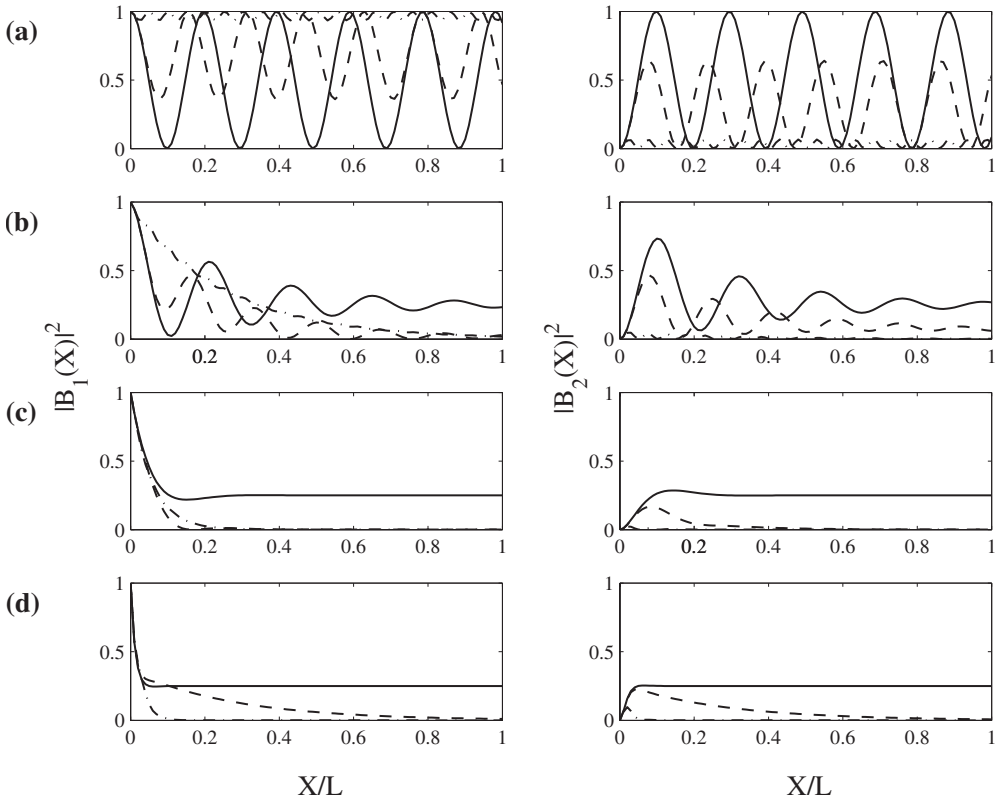

FIG. 8. The transmitted wave intensity $|B_1(X)|^2$ (left) and the scattered wave intensity $|B_2(X)|^2$ (right) over the cylinder array of very large width $\frac{\Omega_0 L}{C_g}=8$ for different detuning parameters $\frac{\Omega}{\Omega_0}=0$ (solid curve), 1 (dashed curve), and 5 (dash-dotted curve): (a) $\Lambda a=0.0$ (no dissipation), (b) $\Lambda a=0.1(1+\mathrm{i})$, (c) $\Lambda a=0.5(1+\mathrm{i})$, and (d) $\Lambda a=2.0(1+\mathrm{i})$.

The boundary conditions are

$$B_1^- = B_1, \quad X=0 \quad \text{and} \quad B+ = B^+, \quad B_2 = B_2^+, \quad X=L. \tag{6.12}$$

For these (β_1, β_2), the real and imaginary parts of the two eigenvalues ξ_1 and ξ_2 are displayed in Fig. 7 for different values of the dissipation parameter Λa and for a range of the detuning parameter $\frac{\Omega}{\Omega_0}$. In the absence of viscosity, both eigenvalues are real [see Fig. 7(a)], but complex otherwise. The imaginary part is larger for greater viscosity.

The amplitudes in the open water on the incidence side are

$$B_1^-(X) = e^{\mathrm{i}\mathcal{K}\cos\beta_1 X}, \quad B_2^-(X) = 0; \quad X<0. \tag{6.13}$$

Imposing the two matching conditions at $X=0$—$B_1(0)=1$ and $B_2(0)=0$—we find

$$B_1(X) = \frac{M_{11}-\xi_2}{\xi_1-\xi_2}\exp\left[\frac{\mathrm{i}\xi_1\Omega_0 X}{C_g}\right] - \frac{M_{11}-\xi_1}{\xi_1-\xi_2}\exp\left[\frac{\mathrm{i}\xi_2\Omega_0 X}{C_g}\right], \tag{6.14a}$$

$$B_2(X) = \frac{(M_{11}-\xi_1)(M_{11}-\xi_2)}{M_{12}(\xi_1-\xi_2)} \times\left\{-\exp\left[\frac{\mathrm{i}\xi_1\Omega_0 X}{C_g}\right] + \exp\left[\frac{\mathrm{i}\xi_2\Omega_0 X}{C_g}\right]\right\}. \tag{6.14b}$$

These are formally the same as Eqs. (72), (73a) and (73b) in [2] with the new ξ_i and M_{ij} given above.

The wave intensities $|B_1(X)|^2$ and $|B_2(X)|^2$ across the array are shown in Fig. 8 for $\Omega_0 L/C_g=8$. As the detuning parameter Ω/Ω_0 increases, the scattered wave becomes weaker. Spatial oscillations of both $|B_1(X)|^2$ and $|B_2(X)|^2$ become more intense as detuning increases, but disappear as Λa increases. Without dissipation one finds, at certain X_n/L, $B_1(X_n)=1$ and $B_2(X_n)=0$. Therefore transmission is perfect if the array width is exactly X_n. On the other hand, at certain other X_m/L, $B_1(X_m)=0$, while $B_2(X_m)=1$; only the scattered wave is seen at the exit if the array width is exactly X_m. Now on the transmission side only the scattered wave emerges, which can be viewed as a transmitted wave inclined at the angle $\beta_2=-\pi/3$. In this particular case the array behaves not like a piece of transparent glass, but like a mirror transverse to the array and reflects the incident waves. With increasing viscosity, this occurrence is weakened.

To examine the effect of detuning on the waves at the exit edge, we fix the array width L. The dependence of $|B_1(L)|^2$

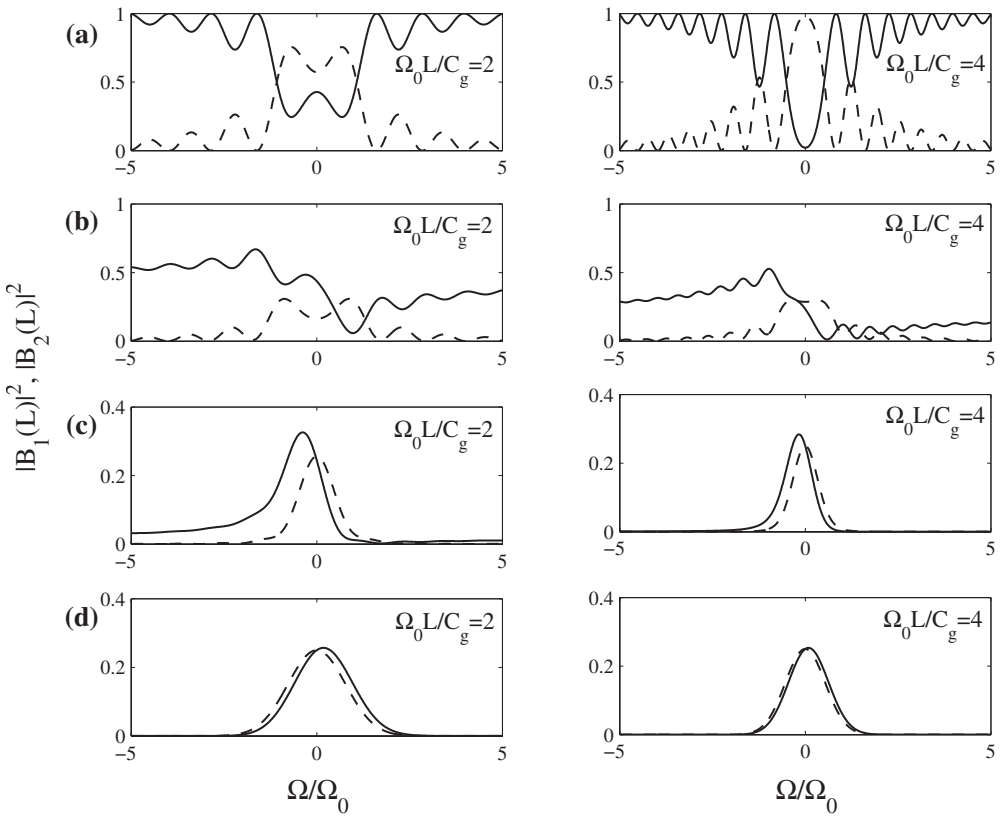

FIG. 9. Dependence of transmitted wave intensity $|B_1(L)|^2$ (solid curve) and forward-scattered wave intensity $|B_2(L)|^2$ (dashed curve) on the detuning $\frac{\Omega}{\Omega_0}$ for strip width $\frac{\Omega_0 L}{C_g}=2$ (left) and $\frac{\Omega_0 L}{C_g}=4$ (right). Inside the strip, the two resonated wave vectors are inclined at $\beta_1=\frac{\pi}{3}$, $\beta_2=-\frac{\pi}{3}$. (a) $\Lambda a=0.0$ (no dissipation), (b) $\Lambda a=0.1(1+i)$, (c) $\Lambda a=0.5(1+i)$, and (d) $\Lambda a=2.0(1+i)$. Different scales are used for the ordinates.

and $|B_2(L)|^2$ on the detuning frequency $\frac{\Omega}{\Omega_0}$ is plotted for two array widths $\Omega_0 L/C_g=2$ and 4 in Fig. 9. Without dissipation, transmission is small, but scattering is strong in the inviscid band gap centered around $\Omega=0$. With dissipation, the band gap disappears. For small $\Lambda a=0.1(1+i)$, transmission and scattering are both weakened. With larger dissipation, the two forward waves become equally small and significant only near $\Omega=0$.

C. Backward scattering: $\cos\beta_2<0$

As another example, we consider a square lattice of spacing a_1 and choose the incident wave vector $\mathbf{k}_1$ such that the scattered wave vector $\mathbf{k}_2$ is as shown in Fig. 10—i.e., $\beta_1=\pi/6$—so that $\beta_2=5\pi/6$. The incident wave number is $k=2\pi/\sqrt{3}a_1$. Now the boundary conditions at the edges of the cylinder array are

$$B_1(0)=1, \quad B_2(L)=0. \tag{6.15}$$

The solutions are formally the same as Eqs. (98)–(100) in [2].

For these angles (β_1,β_2), the real and imaginary parts of the complex ξ_1 and ξ_2 are shown for a range of detuning Ω/Ω_0 and different values of λa in Fig. 11. Understandably, the qualitative features are similar to the one-dimensional case of normal incidence and reflection. Without viscosity $\Lambda a=0.0$, there is a band gap. With finite dissipation, both eigenvalues are complex for all Ω/Ω_0. The band gap disappears.

Figure 12 shows the spatial variation of the transmission intensity $|B_1(X)|^2$ and the reflection intensity $|B_2(X)|^2$ across the strip for various detunings $\frac{\Omega}{\Omega_0}=0.5,2,-3$. When $\Lambda a=0.0$, the wave intensities are oscillatory in X for $\Omega/\Omega_0=-3$ and 2 which are outside the band gap, and attenuate monotonically for $\Omega/\Omega_0=0.5$, which is inside the band gap. Understandably, the solutions are qualitatively similar to the one-dimensional case of simple reflection. When $\Lambda a\neq 0.0$,

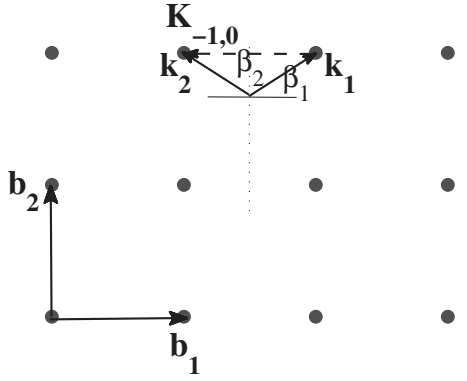

FIG. 10. Backward Bragg scattering by a square lattice of spacing a_1. The incident wave angle $\beta_1=\pi/6$ and the scattered wave angle $\beta_2=\pi-\beta_1=5\pi/6$. The wave number is $k=2\pi/\sqrt{3}a_1$.

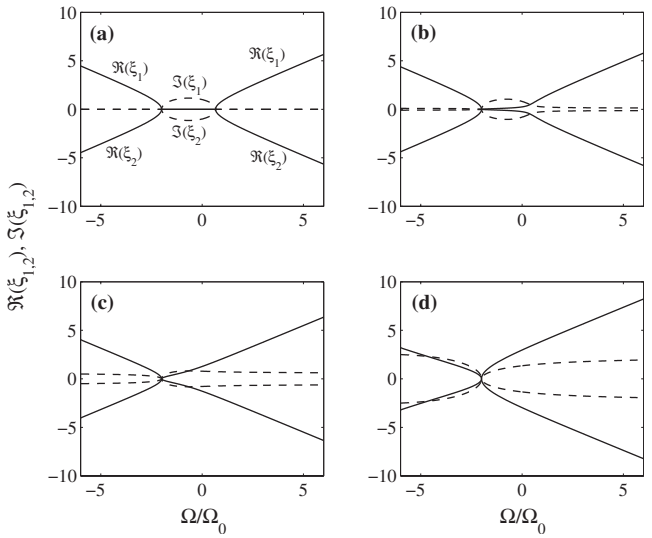

FIG. 11. Dependence of real (solid curve) and imaginary (dashed curve) parts of the eigenvalues ξ_1 and ξ_2 on detuning frequency $\frac{\Omega}{\Omega_0}$ for the backward-scattered waves shown in Fig. 10: (a) $\Lambda a=0.0$ (no dissipation), (b) $\Lambda a=0.1(1+\mathrm{i})$, (c) $\Lambda a=0.5(1+\mathrm{i})$, and (d) $\Lambda a=2.0(1+\mathrm{i})$.

dissipation damps out the oscillations outside the band gap and makes them disappear as Λa becomes larger. Within the band gap, wave intensities attenuate monotonically, but faster as Λa increases.

Figure 13 shows the dependence of transmission intensity at the exit edge $X=L$ (left) and the reflection intensity at the entry edge $X=0$ (right) on the detuning $\frac{\Omega}{\Omega_0}$ for different array widths: $\frac{\Omega_0 L}{C_g}=1,2,8$. Without viscosity, weak tramsmission and strong backscattering prevail inside a clear band gap. With increasing viscosity the band gap shrinks to the immediate neighborhood of $\Omega/\Omega_0=-2$. The transmission intensity diminishes more rapidly than reflection.

VII. CONCLUDING REMARKS

We have examined the effects of viscosity on the propagation of small-amplitude water waves through a periodic array of vertical cylinders. Under the assumptions likely realistic for future offshore airports—i.e., small cylinders and large spacing—we have considered the phenomenon of Bragg resonance. The asymptotic approach of [1,2] is followed. Boundary layer effects due to viscosity are represented in terms of the velocity potential by using a fictitious boundary condition on the cylinders. The effective coefficient is chosen so as to give the correct dynamical effect on the cylinders. The model should be directly applicable to laboratory tests where molecular viscosity is relevant. In the field the boundary layer is likely turbulent so that a much larger (empirical) value of eddy viscosity must be used instead. We also reason in the Appendix that vortex shedding is important only for large-amplitde waves. Since the mathematical problem treated here is similar to two-dimensional scattering of sound by a periodic array of parallel wires, the present theory may be modified to examine the effects of dissipation on multiple scattering including band gaps, etc.

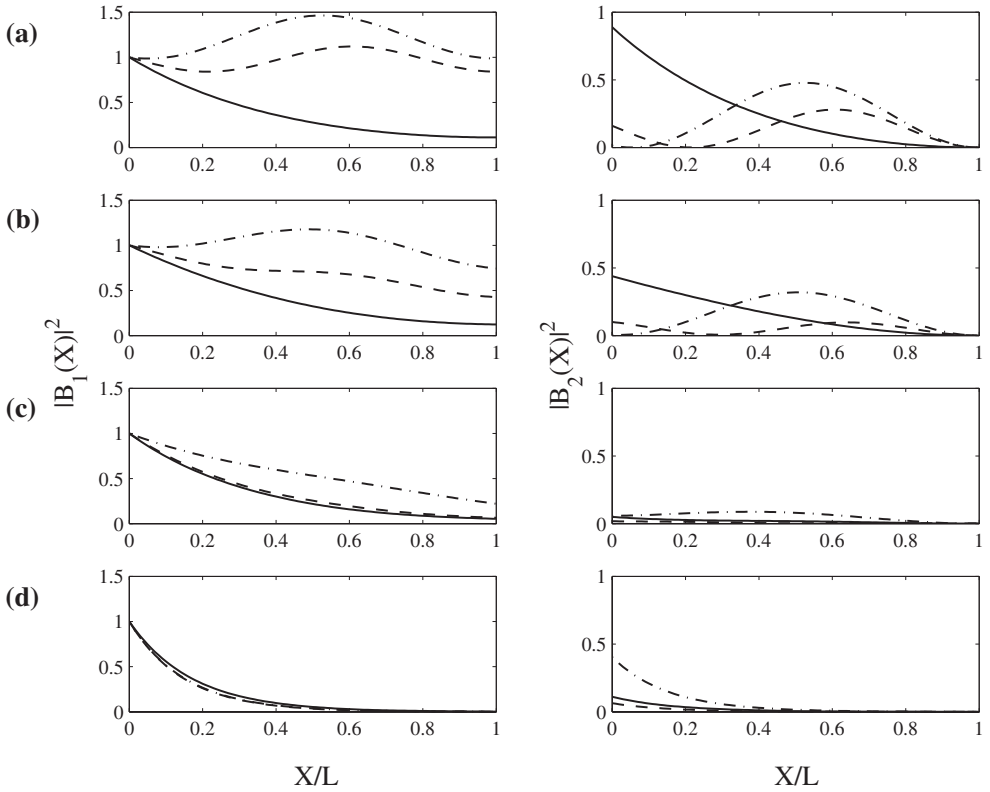

FIG. 12. Transmission intensity $|B_1(X)|^2$ (left) and the reflection intensity $|B_2(X)|^2$ (right) across the strip for various detuning frequencies $\Omega/\Omega_0=0.5$ (solid curve), 2 (dashed curve), and −3 (dash-dotted curve) for the scattering configuration in Fig. 10. The dimensionless strip length is $\Omega_0 L/C_g=2$. (a) $\Lambda a=0.0$ (no dissipation), (b) $\Lambda a=0.1(1+\mathrm{i})$, (c) $\Lambda a=0.5(1+\mathrm{i})$, and (d) $\Lambda a=2.0(1+\mathrm{i})$.

ACKNOWLEDGMENTS

This research was supported by a grant from Masdar Institute of Science and Technology, as a part of the MIT-Abu Dhabi Alliance Program. C.C.M. also received partial support from the U.S.-Israel Binational Science Foundation.

APPENDIX: REMARKS ON VORTEX SHEDDING

As is well known, flow around a smooth vertical circular cylinder in waves is characterized by the Reynolds number ($\mathrm{Re}=U_0D/\nu$) and the Keulegan-Carpenter number [$K_C=U_0T/D$, where U_0 is the horizontal fluid velocity at the center of the cylinder in the absence of the cylinder, T the wave period, D the cylinder diameter, and ν kinematic viscosity (see, for example, [10,11])].

To examine the role of shedding vortices in gentle waves considered here, we focus attention on the free surface ($z=0$) where the horizontal fluid velocity attains its maximum value.

In view of (2.5) and (2.7), the order of magnitude of the horizontal velocity at the free surface can be estimated by

$$|U(x,y,z=0,t)| = |\nabla \eta Z(0)| = \frac{g}{\omega}|\mathrm{Re}\,\nabla\,\eta| = \epsilon\frac{g}{\omega}, \quad \text{(A1)}$$

where $\epsilon=O(\nabla\eta)$ is the measure of local wave steepness. Making use of (2.8) and $\mu=ka$, the maximum of Reynolds and Keulegan-Carpenter numbers at the free surface are

$$\mathrm{Re}_{\max} = \frac{U(z=0)|_{\max}D}{\nu} = \frac{2a}{\nu}\frac{g}{\omega}\epsilon, \quad \text{(A2a)}$$

$$(K_C)_{\max} = \frac{U(z=0)|_{\max}T}{D} = \pi\frac{g}{a\omega^2}\epsilon = \frac{\pi}{\mu}\frac{\epsilon}{\tanh kH}. \quad \text{(A2b)}$$

The linearized asymptotic theory in [1,2] is valid if the wave steepness is small enough such that

$$\epsilon \leqslant O(\mu^2 = k^2a^2) \quad \text{(A3)}$$

(see [1]). Within the realm of the linearized theory, we have the following:

$$\mathrm{Re}_{\max} \leqslant \frac{2a}{\nu}\frac{g}{\omega}O(\mu^2), \quad (K_C)_{\max} \leqslant \frac{\pi}{\tanh kH}O(\mu), \quad \text{(A4)}$$

in view of (A2) and (A3). Note that the maximum of Keulegan-Carpenter number is $O(\mu)$.

Now let us estimate $\mathrm{Re}_{\max}$ and $K_{C_{\max}}$ in reality. In the field, the typical values are $a\sim 1-5$ m, $ka\approx 0.1$, and $kH=1$, which for $\nu=10^{-6}$ m^2/s leads to the following:

$$\mathrm{Re}_{max} \leqslant (0.23-2.5)\times 10^6, \quad (K_C)_{\max} \leqslant 0.41. \quad \text{(A5)}$$

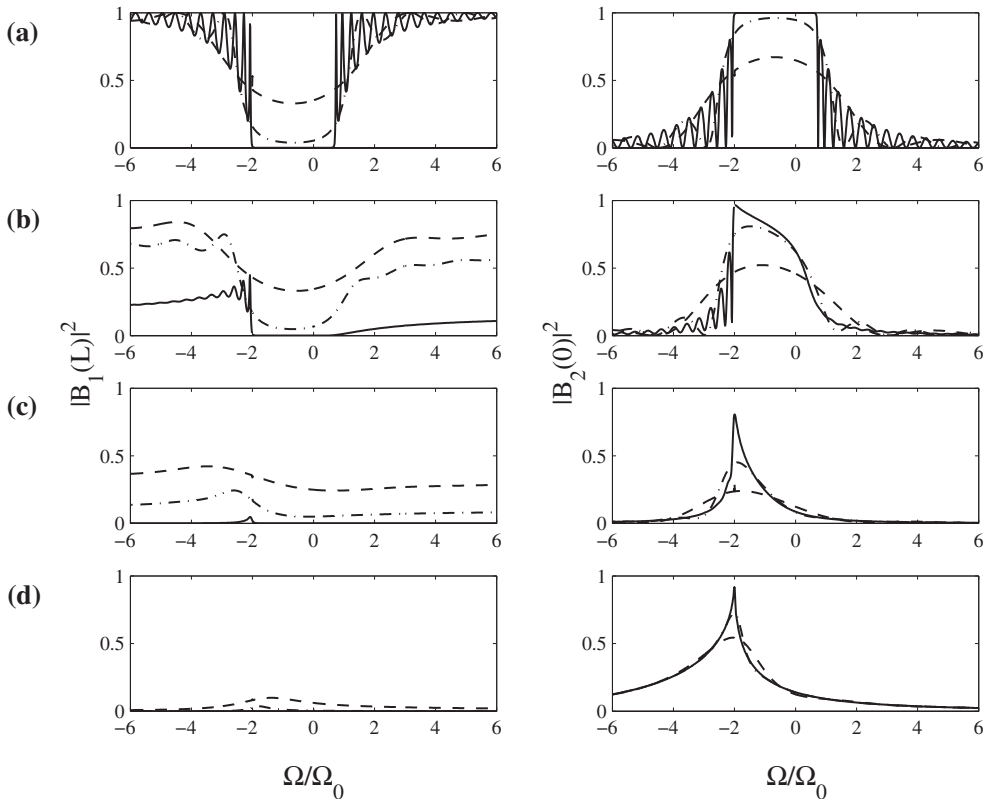

FIG. 13. Transmission intensity $|B_1(L)|^2$ at the exit edge of array (left) and reflection intensity $|B_2(0)|^2$ at the incident edge of array (right) for various detuning Ω/Ω_0 and array widths. Dashed curve: $\Omega_0L/C_g=1$. Dash-dot curve: $\Omega_0L/C_g=2$. Solid curve: $\Omega_0L/C_g=8$. (a) $\Lambda a=0.0$ (no dissipation), (b) $\Lambda a=0.1(1+\mathrm{i})$, (c) $\Lambda a=0.5(1+\mathrm{i})$, and (d) $\Lambda a=2.0(1+\mathrm{i})$.

In laboratory experiments, on the other hand, we take $a \sim 5-25$ cm, $ka \approx 0.1$, and $kH=1$ so that

$$\mathrm{Re}_{max} \leqslant (0.25-2.8)\times 10^4, \quad (K_C)_{\max} \leqslant 0.41. \quad \text{(A6)}$$

According to typical field data (see, e.g., Fig. 3.16) of [11], for Reynolds numbers in the above range for the field, $(0.23-2.5)\times 10^6$, the Keulegan-Carpenter number has to be greater than about 5.4 for vortex shedding to occur. From laboratory tests (see Fig. 3.15 of [11]), for Reynolds number in the range $(0.25-2.8)\times 10^4$, the Keulegan-Carpenter number has to be above 7 to trigger vortex shedding. Both values of the Keulegan-Carpenter number are higher than the estimated values in (A5) and (A6). Hence, within the bounds of linearized theory, vortex shedding is ineffective. For very strong waves, nonlinearity and vortex shedding can of course be important and even overwhelm Bragg scattering. A very different theory is then needed.

[1] Y. Li and C. C. Mei, J. Fluid Mech. **583**, 161 (2007).

[2] Y. Li and C. C. Mei, Phys. Rev. E **76**, 016302 (2007).

[3] C. C. Mei, M. Stiassnie, and D. K. P. Yue, *Theory and Applications of Ocean Surface Waves* (World Scientific, Singapore, 2005).

[4] J. W. S. Rayleigh, Philos. Mag. **12**, 81 (1881).

[5] H. Kagemoto, M. Murai, M. Saito, B. Molin, and S. Malenica, J. Fluid Mech. **456**, 113 (2002).

[6] This fictitious condition can also be applied to two-dimensional sound scattering by thin wires. Take, for example, the sound frequency $f=\omega/2\pi=10$ kHz, so that $\omega=2\pi\times 10^2$ rad/s. The Stokes boundary layer thickness is $\delta=0.707\times 10^{-3}$ cm. For a fiber radius of 0.1 cm, we get $\bar{\Lambda}a \sim 0.01$ which is also small.

[7] N. W. Aschcroft and N. D. Mermin, *Solid State Physics* (Thomson Learning Inc., 1976).

[8] C. Kittel, *Introduction to Solid State Physics*, 8th ed. (Wiley, New York 2004).

[9] In Sec. IV A and Appendix B of [2], z^2 everywhere should be changed to $|Z|^2$.

[10] T. Sarpkaya and M. Isaacson, *Mechanics of Wave Forces on Offshore Structures* (Van Nostrand Reinhold, New York, 1981).

[11] B. M. Sumer and J. Fredsoe, *Hydrodynamics Around Cylindrical Structures* (World Scientific, Singapore, 1997).